SCIENCE CHINA
Technological Sciences

Special Topic: Mechanical Behaviour of Micro- and Nano-Scale Materials
• Article •

April 2014 Vol.57 No.4: 663–670
doi: 10.1007/s11431-014-5498-0

An index for deformation controllability of small-volume materials

WANG ZhangJie[1*], SHAN ZhiWei[1], LI Ju[1,2*], SUN Jun[1] & MA Evan[1,3]

[1]*Center for Advancing Materials Performance from the Nanoscale (CAMP-Nano) & Hysitron Applied Research Center in China (HARCC), State Key Laboratory for Mechanical Behavior of Materials, Xi'an Jiaotong University, Xi'an 710049, China;*
[2]*Department of Nuclear Science and Engineering and Department of Materials Science and Engineering, Massachusetts Institute of Technology, Cambridge, Massachusetts 02139, USA;*
[3]*Department of Materials Science and Engineering, Johns Hopkins University, Baltimore, Maryland 21218, USA*

Received January 16, 2014; accepted February 28, 2014

Mechanical tests on small-volume materials show that in addition to the usual attributes of strength and ductility, the controllability of deformation would be crucial for the purpose of precise plastic shaping. In our present work, a "mechanical controllability index" (MCI) has been proposed to assess the controllability of mechanical deformation quantitatively. The index allows quantitative evaluation of the relative fraction of the controllable plastic strain out of the total strain. MCI=0 means completely uncontrollable plastic deformation, MCI=∞ means perfectly controllable plastic shaping. The application of the index is demonstrated here by comparing two example cases: 0.273 to 0.429 for single crystal Al nanopillars that exhibit obvious strain bursts, versus 3.17 to 4.2 for polycrystalline Al nanopillars of similar size for which the stress-strain curve is smoother.

mechanical controllability index, plastic deformation, strain bursts, nanomechanics

Citation: Wang Z J, Shan Z W, Li J, et al. An index for deformation controllability of small-volume materials. Sci China Tech Sci, 2014, 57: 663–670, doi: 10.1007/s11431-014-5498-0

1 Introduction

Metalworking is a cornerstone of civilization, with widespread applications from beer cans to automobile bodies. The ability of metals to be cold-formed into complex shapes depends on two crucial attributes: ductility and controllability of plastic deformation. Ductility is well known: it characterizes the largest achievable plastic strain before fragmentation and utter failure [1]. The second attribute, controllability, characterizes whether an arbitrary plastic strain within the maximum achievable plastic strain can indeed be practically imparted in a controlled manner.

Controllability turns out to be a serious problem for micro- and nano-scale metallic components. For example, ductile metals such as Au and Al, in bulk form, are well known to have smooth stress-strain curves, exhibit continuous work hardening and offer excellent controllability in shaping and forming. However, these highly desirable features are not necessarily present when the free-standing single crystal approaches submicron-size. Recently through quantitative testing, the small volume metals, such as the single-crystal micro- and nano-pillars, show that the plastic flow is characterized by pronounced displacement bursts long before gross failure, even though they provide high strength following the "smaller is stronger" trend [2–14]. Examples of such behavior will be presented in Section 3 below. These intermittent plastic events are due to collective dislocation activities [15], rather than the slip of each individual dislocation. Note that even though collective dislocation avalanches are also present when deforming bulk samples, their effect is much amplified in small-volume materials because each avalanche now contributes

*Corresponding authors (email: zhangjiewang@mail.xjtu.edu.cn, liju@mit.edu)

larger overall strain and shape change to the sample (especially when the object dimension is on nanoscale). Some large displacement bursts can cause the sample to undergo sudden "structural collapse" without warning. Here the phrase "structural collapse" refers to large, unpredictable and abrupt change in sample shape; in some cases, the sample turns into a pancake in such a collapse [16–18]. In other cases, major offsets due to shear events localized on particular crystallographic planes appear on the sides of the deforming pillar [3]. Structural collapse renders major shape changes abrupt, random (in terms of when and where it happens) and step-like, and thus difficult/impossible to control.

So far, there is no quantitative way to evaluate how controllable the plastic strain is. In Section 3 that follows, through quantitative nanomechanical testing inside a transmission electron microscope (TEM), we will first demonstrate two cases of Al nanopillars showing different controllability of plastic deformation. We will then introduce in Section 4 a new mechanical controllability index (MCI), and illustrate its use in Section 5 by quantitatively assessing the degree of controllability for these two example cases.

2 Experimental method

The single crystal Al nanopillars have taper angles of about 2° and nominal free end diameters (D) ranging from 100 to 406 nm, typically having an aspect ratio around 2.5. They were fabricated from a piece of Al single crystal slice using an FEI Dual Beam focused ion beam (FIB) system. The starting Al slice had a thickness of 200 μm and a diameter of 3 mm. Then it was mechanically polished on both sides to a thickness of 50 μm. One edge of the slice was then subjected to twin-jet polishing to obtain a thin region with several micrometers in thickness, in a chemical solution of methanol with 5% perchloric acid. In the thinned region, pillars with different diameters were fabricated at an ion-beam accelerating voltage of 30 keV, with the beam current gradually decreasing from 0.28 nA to 1.5 pA. Finally the single crystal Al nanopillars were cleaned using the planar scanning mode of ion beam working at 5 keV and 1.5 pA. High resolution TEM observation of the Al nanopillars fabricated under the above conditions shows that the surface amorphous layer is only around 1 nm.

The polycrystalline Al nanopillars were made from polycrystalline Al thin films, which were deposited at room temperature using magnetron sputtering onto a silicon substrate that includes a narrow wedge, as described elsewhere [19]. The base vacuum is 4.6×10^{-8} mbar. The argon working pressure is 5.3×10^{-3} mbar. They were then annealed in the vacuum chamber at 467 K ($0.5T_m$) to stabilize the grain structure. The polycrystalline Al nanopillars with nominal free end diameters of 108, 141, and 190 nm were then prepared via FIB micromachining, using similar parameters as those for single crystal nanopillars.

The quantitative compression tests were carried out using a Hysitron PI95 TEM PicoIndenter inside a JEM 2100 field emission gun TEM. The core part of this nanomechanical testing system is the force/displacement transducer developed by Hysitron Inc. [20]. It provides high sensitivity and large dynamic range with maximum force up to 1.5 mN and a linear displacement output up to 5 μm. All compression tests were carried out under displacement rate control mode due to its greater sensitivity to transient phenomena [21]. The nominal strain rate is of the order of 10^{-2} s^{-1}. The dynamic deformation process was recorded using a Gatan830 (SC200) CCD camera. It allows one-to-one correlation between the microstructural/geometry evolution and the mechanical data in real time.

3 Experimental results: examples of different controllability

We first present in Figure 1(a) examples of intermittent

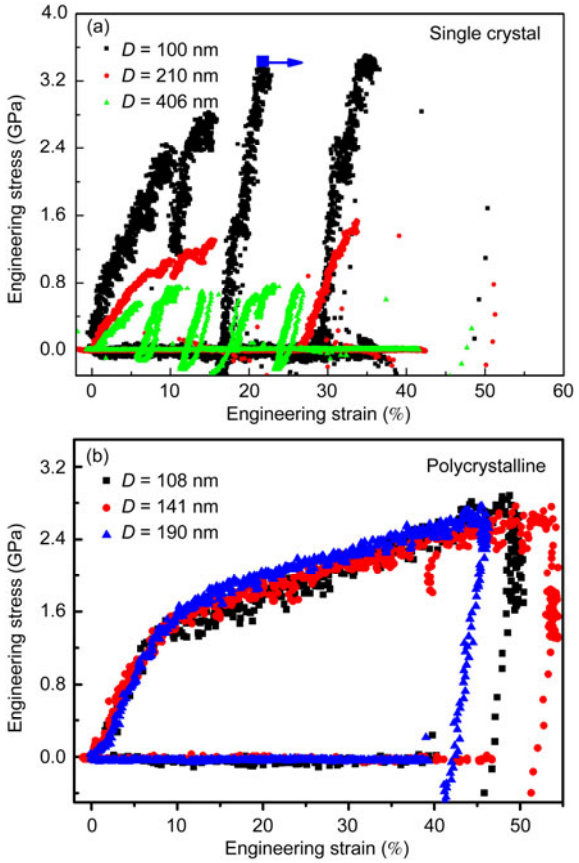

Figure 1 The compression results of Al single crystal nanopillars and Al polycrystalline nanopillars. (a) Engineering stress vs. engineering strain of Al single crystal nanopillars with diameter D = 100, 210, and 406 nm. The marked arrow is a large strain burst. (b) Engineering stress vs. engineering strain of Al polycrystalline nanopillars with D=108, 141, and 190 nm. The nominal loading strain rate is of the order of 10^{-2} s^{-1}.

plasticity for nanoscale single crystal Al nanopillars. The engineering stress (force divided by the cross sectional area calculated based the nominal free end diameter) is much higher than bulk Al, approaching 3 GPa for the smaller (D=100 nm) nanopillar. This is consistent with the "smaller is stronger" trend. It is worth noting that the calculated engineering stress overestimated the maximum stress of the nanopillar because the gradually increased nanopillar diameter in response to the plastic deformation. For each of the three nanopillars tested, the stress-strain curve shows multiple stress serrations and strain bursts. As seen in Figure 1(a), for some serrations the load drop is so large that the stress reaches zero. The negative forces seen in Figure 1(a) are due to the adhesion force between the diamond flat punch and the sample.

The *in situ* real-time monitoring inside the TEM allows direct correlation between the intermittent plasticity in the stress-strain response and the corresponding changes in the microstructure and morphology of the sample. The as-fabricated Al nanopillar with a D=100 nm was shown in Figure 2(a). FIB-introduced defects and pre-existing dislocations can be clearly seen. These defects can be eliminated through the application of "mechanical annealing" [21], leading to a sample interior that is almost dislocation free with the proceding of compression. The nanopillar is loaded along the $[1\bar{3}1]$ direction as revealed by the diffraction pattern ([211] zone axis) in Figure 2(b). Figures 2(c) and (d) are snapshots acquired during the compression process of the D=100 nm nanopillar (see the movie in the supporting information). It compares the nanopillar before and after a large burst (marked by the blue arrow in Figure 1(a)). These two images were taken 0.2 s apart, indicating a rapid change in sample height and shape during this abrupt instability event. These large displacement bursts are widely observed in single crystal nanopillars. It results in abrupt structural collapse: along the compression direction the displacement jump is larger than tens of nanometers in less than 0.2 s. Bursts up to 100 nm have been seen in other samples and by other groups in other metals [16,22,23].

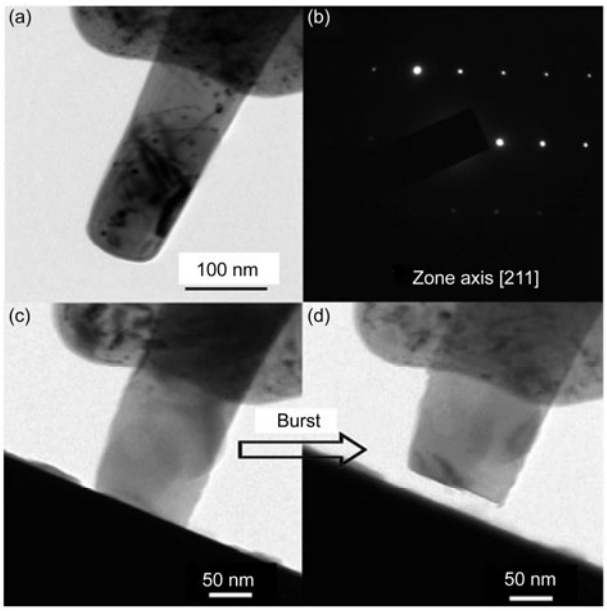

Figure 2 (See Movie S1 in supporting information) *In situ* compression along the $[1\bar{3}1]$ direction of Al single-crystal nanopillar with D=100 nm. (a) Bright-field image of the nanopillar before compression. (b) The diffraction pattern in [211] zone axis. From (c) to (d) shows the uncontrollable structural collapse during the large strain burst marked in Figure 1(a).

The intermittent plasticity is believed to arise from the jerky motion of dislocations [24], particularly their collective actions in groups [25]. Csikor et al. [15] envisioned the intermittent plastic flow as stemming from the following mechanism: multiple dislocations are trapped into "jammed configurations", and "the long-range mutual interaction between dislocations" makes "the destruction of such jammed configurations a collective and avalanche-like process". A pre-requisite for a sudden and major pillar shape change is therefore the existence, and cooperative motion, of a large population of accumulated dislocations, which burst out of the sample in an avalanche. However, the jammed dislocation configuration is unlikely to exist in nanopillars that can experience mechanical annealing prior to dramatic strain burst. Alternatively, there could be explosive (i.e. sudden and highly correlated) nucleation of dislocations from a large number of dislocation sources, such that numerous dislocations penetrate the sample all at once in a meteor-shower-like event [26].

It has been proposed that the introduction of internal structures, such as grain boundaries, can hinder the dislocation avalanche and therefore improve the controllability of plastic deforming [15]. For example, micro- and nano-scaled polycrystalline pillars [27–29] had been reported to show smoother stress-strain curves and more controllable plastic flow than that of the single crystal nanopillars with similar size. Here in our present work, we show an extreme case in Figure 1(b): an example of almost smooth stress-strain curves resulted from polycrystalline Al nanopillars. For such nanopillars, the stress-strain curves are much smoother than the single crystal nanopillars (compare Figures 1(a) and (b)). It is virtually free of the major serrations and shape collapses. The microstructure of the polycrystalline Al nanopillars are shown in Figure 3. The grains are mostly columnar with width in the 10 to 100 nm range. Apparently, the grain boundaries and defects contained in the sputter-deposited film (see images in Figure 3(a)) served as obstacles to suppress and block the (collective) escape of dislocations and help dislocation storage. Possibly the impurities induced during deposition process also helps to suppress large dislocation avalanches. Throughout the large deformation to ~45% strain, the stress-strain curves remain smooth. The *in situ* TEM observation indicates continuous sample compression and barreling (see the movie in supporting information), without obvious localized bands or

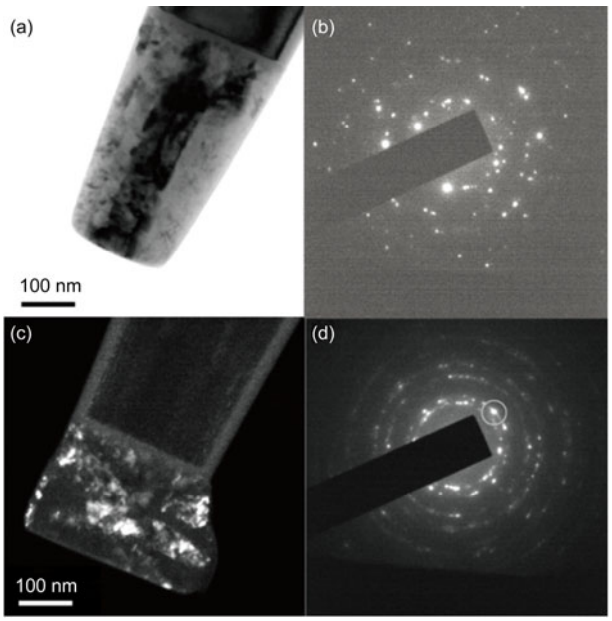

Figure 3 (See also Movie S2 in supporting information) The microstructure of Al polycrystalline pillar with D=190 nm before and after compression. (a) Bright-field image; (b) diffraction pattern of the polycrystalline pillar before compression; (c) and (d) those after compression.

large discrete shear steps (see image in Figure 3(c)). The diffraction pattern in Figure 3(d) suggests that the grain size of the nanopillar was reduced due to the severe plastic deformation. The dark field image in Figure 3(c) shows the finer grains.

From the two examples above, we see that nanopillars of a conventionally very ductile metal, in this case Al, can display quite different degrees of controllability of plastic strains. In the experiments reported so far on various metal pillars, the controllability (or smoothness of the stress-strain curves) ranges from completely smooth behavior all the way to sudden burst that collapses the sample to a pancake right upon yielding [16,17]. The vast majority of the reported curves display strain bursts to various degrees, such as those in Figure 1(a). It is therefore necessary, and at the same time a challenging task, to be able to quantitatively evaluate and compare the degree of controllability of the plastic deformation.

4 The definition of MCI

We now proceed to establish a generally applicable, quantitative index of mechanical controllability. To this end, we first acquire stress (σ)-actual strain (ε)-time (t) data from the load-displacement-time raw data from the nanomechanical device readout. The following procedure is found to be the most robust and effective, in the sense that the result is insensitive to instrument noise and basic material parameters, like Young's modulus, hardness, and strength. First, the effective Young's modulus E is extracted from the final unloading. This allows one to estimate the actual plastic strain (ε_{p}) of the workpiece as a function of time by a "virtual unloading" estimate:

$$\varepsilon_{\mathrm{p}}(t) = \varepsilon(t) - \frac{\sigma(t)}{E}. \tag{1}$$

In situations where large shape changes have occurred and the estimation of unloading E is infeasible, or if it is apparent that the total strain is dominated by the plastic strain, one could approximate $\varepsilon_{\mathrm{p}}(t)$ by $\varepsilon(t)$. Here, one needs to ensure that $\varepsilon_{\mathrm{p}}(t)$ reflects the actual plastic strain of the work piece. Sometimes the indenter is detached from the workpiece after it suddenly collapsed, causing wild adjustments (flagged "too fast") followed by gradual advancement of the indenter with negligible load (flagged "empty load"), before contact is reestablished. These data are automatically identified and removed by a computer program (see the supporting information).

Based on $\varepsilon_{\mathrm{p}}(t)$ trajectory, we calculate the density of (plastic-strain) states (DoS):

$$\rho(\varepsilon) \equiv \int_{t_{\mathrm{start}}}^{t_{\mathrm{finish}}} \mathrm{d}t\,\delta(\varepsilon - \varepsilon_{\mathrm{p}}(t)), \tag{2}$$

where $\delta()$ is the Dirac delta function, and t_{start}, t_{finish} are the begin and finish times of the experiment (the corresponding plastic strains are $\varepsilon_{\mathrm{Pstart}}$, $\varepsilon_{\mathrm{Pfinish}}$). An actual $\varepsilon_{\mathrm{P}}(t)$ trajectory is of course in discrete-sample form $\{\varepsilon_{\mathrm{P}}^{(k)}, t^{(k)}\}$ in real measurements, and one evaluates eq. (2) numerically by a histogram approach, assuming the trajectory between $(\varepsilon_{\mathrm{P}}^{(k)}, t^{(k)}) - (\varepsilon_{\mathrm{P}}^{(k+1)}, t^{(k+1)})$ is linear. Eq. (2) is inspired by the density-of-states definition in solid-state physics, with "energy" replaced by "plastic strain". The spectrum $\rho(\varepsilon_{\mathrm{P}})$ has unit of time/strain, and reflects how much net dwell time the system spends in the plastic strain range $(\varepsilon_{\mathrm{P}}, \varepsilon_{\mathrm{P}} + \mathrm{d}\varepsilon_{\mathrm{P}})$. We then define the span of "controllable plastic strain" $\varepsilon_{\mathrm{P}}^{\mathrm{control}}$ by

$$\varepsilon_{\mathrm{P}}^{\mathrm{control}} \equiv \int \mathrm{d}\varepsilon_{\mathrm{P}}\Theta(\rho(\varepsilon_{\mathrm{P}}) - \mathrm{CSR}^{-1}), \tag{3}$$

where $\Theta()$ is the Heaviside step function ($\Theta(x>0)=1$, $\Theta(x\leqslant 0)=0$), and CSR is a "critical strain rate" parameter, presently set to be CSR = 0.1/second to symbolize possible machine response time. In other words, those plastic strain states where the dwell time density is less than CSR^{-1} are defined as inaccessible to an automatic machine. (2), (3) are essentially a numerical approach to identify those plastic strains covered by "strain bursts", which occurs at a really high strain rate (exceeding CSR) so with the present technology an automatic machine cannot respond quickly enough to "lock in" and utilize those plastic strains for shaping purposes. The reason

$\varepsilon_{\mathrm{P}}^{\mathrm{control}}$ is identified via eqs. (2) and (3), rather than the more straightforward manner based on $\mathrm{d}\varepsilon_{\mathrm{P}}/\mathrm{d}t = (\varepsilon_{\mathrm{P}}^{(k+1)} - \varepsilon_{\mathrm{P}}^{(k)})/(t^{(k+1)} - t^{(k)})$ is because unlike in conventional macroscopic material measurements, there is so much noise in the nanomechanical $\{\varepsilon_{\mathrm{P}}^{(k)}, t^{(k)}\}$ that $\mathrm{d}\varepsilon_{\mathrm{P}}/\mathrm{d}t$ often has negative value ("re-entrant"). To obtain a sensible $\varepsilon_{\mathrm{P}}^{\mathrm{control}}$ estimate with an algorithm that is not sensitive to the noises and data sampling rate, eqs. (2) and (3) is the best approach we have discovered so far.

Armed with the spectrum of controllable strain, the mechanical controllability index (MCI) is simply defined as

$$\mathrm{MCI} \equiv -\ln\left(1 - \frac{\varepsilon_{\mathrm{P}}^{\mathrm{control}}}{|\varepsilon_{\mathrm{Pfinish}} - \varepsilon_{\mathrm{Pbegin}}|}\right), \tag{4}$$

where the denominator is the total range of plastic strain experienced by the work piece. MCI defined by eq. (4) is dimensionless and is independent of the hardness and/or modulus of the material: MCI=0 means completely uncontrollable plastic deformation, MCI=∞ means perfectly controllable plastic shaping. For fair comparison, it is better to compare MCI for different materials in a similar plastic strain span under same testing conditions.

5 Calculation of the MCI for Al nanopillars

In the preceding section, we have defined the physical expression of the MCI which is the fraction of controllable plastic strain over total plastic strain. We used a CSR as a criterion to distinguish the controllable plastic strain with uncontrollable plastic strain. Here we describe the detailed mathematical treatment (via MATLAB, see scripts in the supporting information) to realize such calculation step by step, for the Al nanopillar cases in Figure 1.

Firstly, we need to exclude some data points acquired from the machine. The engineering strain (ε)-engineering stress (σ) is calculated from the acquired force-displacement data. Two kinds of "unreal" data need to be rejected. These are ''too fast'' and ''empty load'' data. Once the strain burst occurs, the nanomechanical punch loses its control in this transient and shoots out at a very fast velocity, causing large errors in the displacement and force readout. Therefore, the data points labeled "too fast" should be excluded. After wild re-adjustments, the tip goes back to its designed position by a proportional-integral-derivative (PID) control. Since MCI depends on the choice of CSR monotonically, an extremely good machine with strict control of tip movement should possess better controllability. Only under a perfect displacement control the materials may be plastically formed with extreme precision. This is also the reason why we used the displacement control mode rather than the load control mode. In our present work, the criterion for the elimination of the ''too fast'' data is the velocity. Using MATLAB scripts, we calculate the arc velocity of each data point by

$$v_{\mathrm{arc}} = \frac{\sqrt[6]{\left(\frac{\varepsilon_{k+1} - \varepsilon_k}{\Delta\varepsilon}\right)^6 + \left(\frac{\sigma_{k+1} - \sigma_k}{\Delta\sigma}\right)^6}}{\frac{t_{k+1} - t_k}{\Delta t}}, \tag{5}$$

where σ is the engineering stress, ε is the total strain, $\Delta\sigma$ is the stress range of the whole deformation process and $\Delta\varepsilon$ is the strain range of the whole deformation range. We set the threshold of the velocity at 200: If the velocity is larger than 200, we treat it as an ''too fast'' data and eliminate it. The threshold for the v_{arc} can be tuned by the practical condition. In present work, 200 is sufficient for our selection of efficient data. The marked data points of ''too fast'' data are shown in Figure 4 by red circle. If the strain burst is large, there exists a gap between the pillar and the tip after it goes back to its legitimate position. The tip will be put forward by the setting program again. Before the tip approached the pillar, it is at an empty-load state, during which the tip displacement also can not indicate the deformation information. The elimination of ''empty load'' is simply done by discarding the data points whose stress value is at the noise level. The noise level for each loading can be read out from the empty-load process. For example, in Figure 4, the noise level is 65 MPa. All the empty-load data points whose stress is lower than 65 MPa were marked by the purple circle.

The next step is to transform the total strain to plastic strain by virtual unloading, since what we need is the plastic strain information:

$$\varepsilon_{\mathrm{p}_k} = \varepsilon_k - \frac{\sigma_k}{E}, \tag{6}$$

where $\varepsilon_{\mathrm{P}k}$ is the plastic strain, ε_k is the total strain, σ_k is the engineering stress and E is the modulus obtained from the real unloading process. The dashed line in Figure 5 is the elastic loading curve drawn by the obtained modulus. Finally, the plastic strain-time data was reformulated in a new data file for the subsequent calculation. See subsection 1 in the supporting information for the MATLAB scripts.

The plastic strain-time curve is shown in Figure 6(a). To distinguish between the controllable plastic strain with uncontrollable plastic strain, we introduce the "visit intensity":

$$I_{\mathrm{v}} = \frac{t_{k+1} - t_k}{\varepsilon_{\mathrm{P}k+1} - \varepsilon_{\mathrm{P}k}}. \tag{7}$$

Imagine we have a "bomber airplane" to visit a plastic strain range $\varepsilon_{\mathrm{P}k+1} - \varepsilon_{\mathrm{P}k}$, I_{v} can be seen as the time it takes the "bomber airplane" to fly over such a plastic strain range as shown in Figure 6(b). If the total dwell time of the "bomber

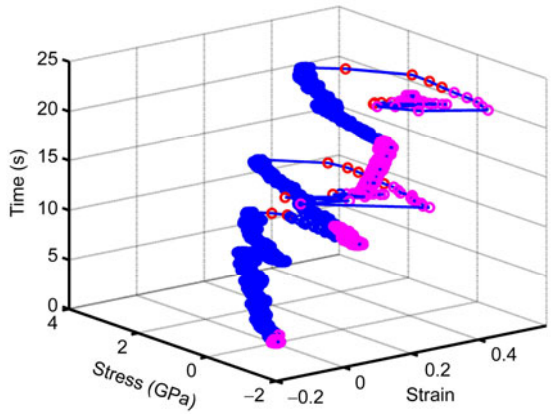

Figure 4 The strain-stress-time curve of the compression of Al single crystal pillar (D=100 nm). Different kinds of data are marked by various colors. The blue ones are the useful data. The red ones are ''too fast'' data. The purple ones are the ''empty load'' data.

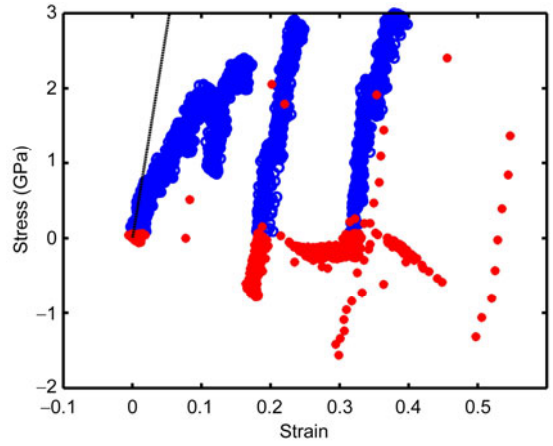

Figure 5 The strain-stress curve of the compression of Al single crystal pillar (D=100 nm). The slope of the dashed line in the figure is the modulus which we will use during virtual unloading.

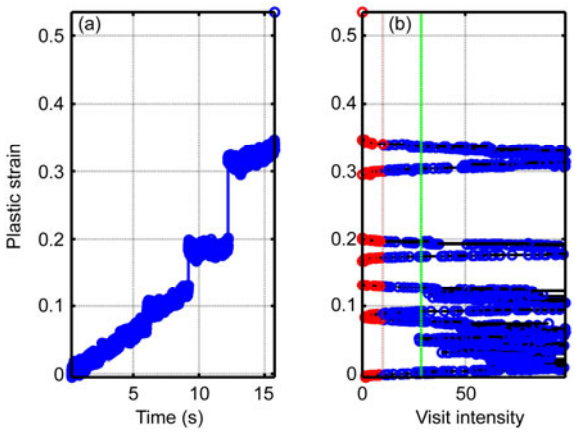

Figure 6 Visit intensity of uncontrollable plastic strain. (a) The plastic strain vs. time curve for the compression of Al single-crystal pillar (D=100 nm); (b) the visit intensity in each plastic strain range. The red circle points are the data lower than 1/CSR. The dashed green line is the average visit intensity.

airplane" over a plastic strain range is too small, it means a controller would not likely be able to "lock in" that particular plastic strain even it wants to do so ("drop a bomb"). So the plastic strains within such a range would be inaccessible. The mathematical expressions in eqs. (2) and (3) are just a numerically robust way to accumulate I_v upon noisy, multiple re-entries. Only when the accumulated I_v (= $\rho(\varepsilon)$ in eq. (2)) is larger than a critical value, can a controller lock in this plastic strain for the purpose of precise mechanical shaping, by unloading to zero stress. The threshold of the accumulated I_v ($\rho(\varepsilon)$) is 1/CSR. We note that the threshold for CSR is determined by the quality of controller, in our present work, it is set to be 0.1/second. With a histogram approach, after accumulating I_v to all the plastic strains experienced from each and every $(\varepsilon_P^{(k)},t^{(k)})-(\varepsilon_P^{(k+1)},t^{(k+1)})$, we locate all the accessible plastic strains. Finally we can calculate MCI which is the fraction of the controllable plastic strain out of the max plastic strain. The MCI for the D=100 nm single crystal Al nanopillar is 0.429 (calculated from the data presented in Figures 4–6). The scripts of the MATLAB program are given in Section 2 of the supporting information. The MCI for single crystal Al nanopillars with D=210 nm and D=406 nm are 0.33 and 0.273, respectively (see Figures S1 and S2 in the supporting information). Figure 7 are the data of an example of Al polycrystalline nanopillar with D=190 nm. Figure 7(a) shows the refining of the acquisition data. And the plastic strain vs. time and the visit density were shown in Figures 7(b) and (c). The calculated MCI is 4.2. The MCIs for another two polycrystalline Al nanopillars are 4.14 for D=108 nm (Figure S3 in the supporting information) and 3.17 for D=141 nm (Figure S4 in the supporting information). Our result indicates that the polycrystalline Al nanopillars has larger MCI than that of Al single nanopillar in the similar size.

For multiple stress-strain curves of a material of nominally the same sample size, one would calculate the MCI for each curve and then average the MCIs, and use the mean and variance of such MCI sampling to characterize the size-dependent material property (rather than averaging the stress-strain curve first and then calculate the MCI). The usage of our index is advantageous over simply inspecting the stress-strain curves for the smoothness, as it allows quantitative assessment of the controllability, enabling systematic characterization of the size dependence of the controllability for the same material, as well as the material dependence of the controllability for a given similar size.

6 Conclusions

We have shown that one can use a quantitative controllability index (MCI) to evaluate how controllable the plastic flow is when deforming a nanoscale object. Very different MCI values, bounded between 0 and ∞, can be

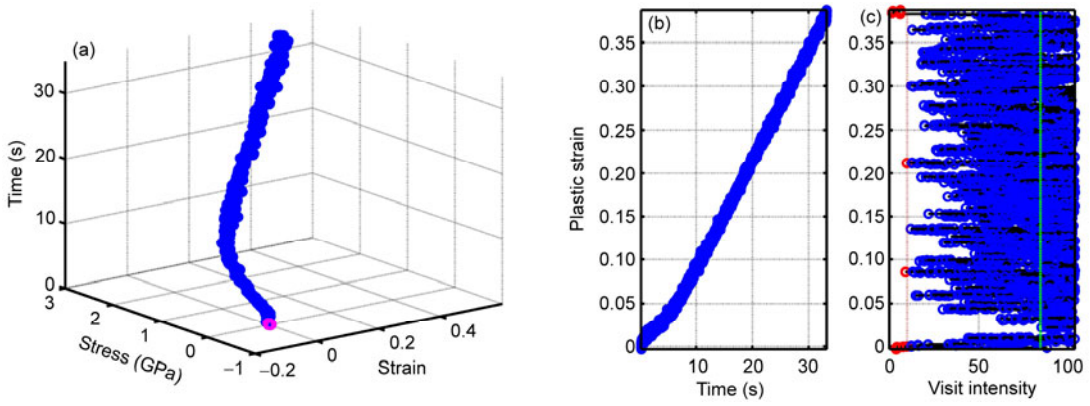

Figure 7 MCI calculation of the D=190 nm polycrystalline Al nanopillar. The color scheme is the same as in Figure 4. (a) Strain-stress-time curve; (b) plastic strain-time curve; (c) visit intensity at each plastic strain range.

obtained for the plastic flow in different nanopillars, as demonstrated here using two examples with very different stress-strain curves. When a smooth stress-strain curve is obtained, such as the ones in Figure 1(b) for nanopillars with polycrystalline internal microstructure, MCI approaches infinity, much like in the deformation of bulk metals. A much reduced MCI, when nanopillars exhibit jerky stress-strain curves containing obvious strain bursts, such as the ones in Figure 1(a). In the extreme cases where the nano-object collapses into a pancake instantly upon yielding, MCI drops nearly to zero. The latter scenario has been widely observed in compression tests of single crystal metals nanopillars, which are of strong current interest worldwide in the study of sample size effects. A dimensionless quantitative controllability index should therefore prove useful in characterizing the plastic flow in these small-volume materials.

This work was supported by the National Natural Science Foundation of China (Grant Nos. 50925104, 11132006, 51231005 and 51321003) and the National Basic Research Program of China ("973" Program) (Grant Nos. 2010CB631003 and 2012CB619402). We also appreciate the support from the "111" Project of China (Grant No. B06025). Both EM and JL carried out this work under an adjunct professorship at XJTU. JL also acknowledges the support by US National Science Foundation (Grant Nos. DMR-1240933 and DMR-1120901).

1 Wang Y M, Chen M W, Zhou F H, et al. High tensile ductility in a nanostructured metal. Nature, 2002, 419: 912–915
2 Brenner S S. Growth and properties of whiskers. Science, 1958, 128: 569–575
3 Uchic M D, Dimiduk D M, Florando J N, et al. Sample dimensions influence strength and crystal plasticity. Science, 2004, 305: 986–989
4 Volkert C A, Lilleodden E T. Size effects in the deformation of sub-micron Au columns. Philos Mag, 2006, 86: 5567–5579
5 Lee S W, Han S M, Nix W D. Uniaxial compression of fcc Au nanopillars on an MgO substrate: The effects of prestraining and annealing. Acta Mater, 2009, 57: 4404–4415
6 Kiener D, Grosinger W, Dehm G, et al. A further step towards an understanding of size-dependent crystal plasticity: *In situ* tension experiments of miniaturized single-crystal copper samples. Acta Mater, 2008, 56: 580–592
7 Richter G, Hillerich K, Gianola D S, et al. Ultrahigh strength single crystalline nanowhiskers grown by physical vapor deposition. Nano Lett, 2009, 9: 3048–3052
8 Frick C P, Clark B G, Orso S, et al. Size effect on strength and strain hardening of small-scale 111 nickel compression pillars. Mater Sci Eng A, 2008, 489: 319–329
9 Ng K S, Ngan A H W. Stochastic nature of plasticity of aluminum micro-pillars. Acta Mater, 2008, 56: 1712–1720
10 Uchic M D, Shade P A, Dimiduk D M. Micro-compression testing of fcc metals: A selected overview of experiments and simulations. JOM, 2009, 61: 36–41
11 Greer J R, Nix W D. Nanoscale gold pillars strengthened through dislocation starvation. Phys Rev B, 2006, 73: 245410
12 Brinckmann S, Kim J Y, Greer J R. Fundamental differences in mechanical behavior between two types of crystals at the nanoscale. Phys Rev Lett, 2008, 100: 155502
13 Bogorosh A, Visniakov N, Novickij J, et al. Dislocation avalanches and strain bursts in the boards of electronic equipment. J Vibroeng, 2013, 15: 233–238
14 Greer J R, De Hosson J T M. Plasticity in small-sized metallic systems: Intrinsic versus extrinsic size effect. Prog Mater Sci, 2011, 56: 654–724
15 Csikor F F, Motz C, Weygand D, et al. Dislocation avalanches, strain bursts, and the problem of plastic forming at the micrometer scale. Science, 2007, 318: 251–254
16 Mook W M, Niederberger C, Bechelany M, et al. Compression of freestanding gold nanostructures: From stochastic yield to predictable flow. Nanotechnology, 2010, 21: 055701
17 Mordehai D, Lee S W, Backes B, et al. Size effect in compression of single-crystal gold microparticles. Acta Mater, 2011, 59: 5202–5215
18 Wang Z J, Shan Z W, Li J, et al. Pristine-to-pristine regime of plastic deformation in submicron-sized single crystal gold particles. Acta Mater, 2012, 60: 1368–1377
19 Minor A M, Morris J W, Stach E A. Quantitative in situ nanoindentation in an electron microscope. Appl Phys Lett, 2001, 79: 1625–1627
20 Warren O L, Shan Z W, Asif S A S, et al. In situ nanoindentation in the TEM. Mater Today, 2007, 10: 59–60
21 Shan Z W, Mishra R K, Asif S A S, et al. Mechanical annealing and source-limited deformation in submicrometre-diameter Ni crystals. Nat Mater, 2008, 7: 115–119
22 Bei H, Shim S, George E P, et al. Compressive strengths of

molybdenum alloy micro-pillars prepared using a new technique. Scrpt Mater, 2007, 57: 397–400
23 Jennings A T, Burek M J, Greer J R. Microstructure versus size: Mechanical properties of electroplated single crystalline Cu nanopillars. Phys Rev Lett, 2010, 104: 135503
24 Petukhov B V. Dynamics of the stochastic jerky motion of dislocations with application to a description of the yield strength anomaly of materials. Mater Sci Eng A, 2004, 387: 98–102
25 Ananthakrishna G. Current theoretical approaches to collective behavior of dislocations. Phys Rep-Rev Sec Phys Lett, 2007, 440: 113–259
26 Wang Z J, Li Q J, Shan Z W, et al. Sample size effects on the large strain bursts in submicron aluminum pillars. Appl Phys Lett, 2012, 100: 071906
27 Pan D, Kuwano S, Fujita T, et al. Ultra-large room-temperature compressive plasticity of a nanocrystalline metal. Nano Lett, 2007, 7: 2108–2111
28 Ng K S, Ngan A H W. Deformation of micron-sized aluminium bi-crystal pillars. Philos Mag, 2009, 89: 3013–3026
29 Dietiker M, Buzzi S, Pigozzi G, et al. Deformation behavior of gold nano-pillars prepared by nanoimprinting and focused ion-beam milling. Acta Mater, 2011, 59: 2180–2192

Supporting information

1 Matlab source code

MatLab scripts for Section 5

2 Supplementary figures

Figure S1 CI calculation for the D=210 nm single-crystal Al pillar. The blue ones are the useful data. The red ones are ‘‘too fast’’ data. The purple ones are the ‘‘empty load’’ data. (a) Strain-stress-time curve; (b) plastic strain-time curve; (c) visit intensity at each plastic strain range.

Figure S2 CI calculation of the D=406 nm single-crystal Al pillar. The color scheme is the same as in Figure S1. (a) Strain-stress-time curve; (b) plastic strain-time curve; (c) visit intensity at each plastic strain range.

Figure S3 CI calculation of the D=108 nm polycrystalline Al nanopillar. The color scheme is the same as in Figure S1. (a) Strain-stress-time curve; (b) plastic strain-time curve; (c) visit intensity at each plastic strain range.

Figure S4 CI calculation of the D=141 nm polycrystalline Al nanopillar. The color scheme is the same as in Figure S1. (a) Strain-stress-time curve; (b) plastic strain-time curve; (c) visit intensity at each plastic strain range.

The supporting information is available online at tech.scichina.com and www.springerlink.com. The supporting materials are published as submitted, without typesetting or editing. The responsibility for scientific accuracy and content remains entirely with the authors.

SCIENCE CHINA
Technological Sciences

Special Topic: Mechanical Behaviour of Micro- and Nano-Scale Materials
• **Article** •

April 2014 Vol.57 No.4: 1–7
doi: 10.1007/s11431-014-5498-0

Supporting information

1 Matlab source code

(1) MatLab scripts for Section 5

```
% NoCrazies.m %
load t_e_sigma_data.txt;
t = t_e_sigma_data (:, 1);
e = t_e_sigma_data (:, 2)/100;
s = t_e_sigma_data (:, 3);

figure (1); clf;
plot3 (e, s, t, '-o'); hold on;
xlabel ('Strain');
ylabel ('Stress [GPa]');
zlabel ('Time [s]');
grid on;

view ([-37.5 20])

trange = max (t)-min (t);
erange = max (e)-min (e);
srange = max (s)-min (s);

exponent = 6;
arcvelocity = ((diff (e)/erange). ^exponent +
(diff (s)/srange). ^exponent). ^ (1/exponent)./ (diff (t)/trange) ;
arcvelocity_threshold = 200;
TooFast = find (arcvelocity > arcvelocity_threshold) + 1;
plot3 (e (TooFast), s (TooFast), t (TooFast), 'ro');
input ('Too fast... eliminate ')

EmptyLoad = find (s < 0.065);
plot3 (e (EmptyLoad), s (EmptyLoad), t (EmptyLoad), 'mo');
input ('Empty load... eliminate ')

Illegitimate = union (TooFast, EmptyLoad);
Legitimate = setdiff (1: length (t), Illegitimate);

print -djpeg StressStrainTime.jpg;

figure (2); clf;
```

*Corresponding author (email: zhangjiewang@mail.xjtu.edu.cn, liju@mit.edu)

```
modulus = 60;
plot (e (Legitimate), s (Legitimate), 'o', ...
        e (Illegitimate), s (Illegitimate), 'r*', ...
        [0 max(s)/modulus], [0 max(s)], 'k--');
xlabel ('Strain');
ylabel ('Stress [GPa]');
question = sprintf ('elastic modulus = %g MPa about right? ', modulus);
input (question)

print -djpeg StressStrain.jpg;

treal = t (Legitimate);
% virtual unloading %
ep = e (Legitimate) – s (Legitimate)/modulus;

LegitimateRecords = length (Legitimate);
for k = 2 : LegitimateRecords,
   if (Legitimate (k) > Legitimate (k-1)+1)
      % there is a break in the Legitimate data %
      treal (k:LegitimateRecords) = treal (k:LegitimateRecords) - ...
            (treal (k)-treal (k-1));
      % rewind the clock spanned by illegitimacy %
      % because it does not reflect evolution of true ep %
   end
end

[maxep, index] = max (e-s/modulus);
if ismember (index, Illegitimate)
% been there, data crazy, but still been there %
   input('max strain achieved during illegitimacy! append data... ')
   treal (LegitimateRecords+1) = treal (LegitimateRecords);
   ep (LegitimateRecords+1) = maxep;
end

data = [treal ep];
save -ascii data.txt data;
figure (3);
TimeBasedControllability;
```

(2) MatLab scripts for Section 5

```
% TimeBasedControllability.m %

% tmin = 0; %
% tmax = 2; %
% tmesh = 10; %
% tdel = (tmax - tmin) / tmesh; %
% t = (tmin: tdel: tmax)'; %
%    %
% AppliedStrainRate = 1e-2; %
% SerrationProb = 0.1; %
%    %
% Jump = (1+2*randn (tmesh, 1))*AppliedStrainRate*tdel; %
```

```
% Idx = find (rand (tmesh, 1) <SerrationProb); %
% Jump (Idx) = Jump (Idx) +AppliedStrainRate*tdel*5; %
%    %
% ep = [0; cumsum (Jump)]; %
% clf; plot (t, ep, 'o'); %
%    %
% data = [t ep]; %
% save -ascii data.txt data; %

% clear all; %
load data.txt;

t = data (:, 1);
ep = data (:, 2);
clf; subplot (1, 2, 1), plot (t, ep, '-o');
xlabel ('Time'); ylabel ('Plastic Strain')
axis ([min (t) max (t) min (ep) max (ep)]);
grid on;

tmesh = length (t) - 1;
Bombing = zeros (tmesh, 1);

[Y, Idx] = sort (ep);

for k = 1: tmesh
   FlyOver = abs ((t (k+1)-t (k)) / (ep (k+1)-ep (k)));
   epbeg = min ([ep (k), ep (k+1)]);
   epend = max ([ep (k), ep (k+1)]);
   range = find ((Y>=epbeg).*(Y<epend));
   Bombing (range) = Bombing (range) + FlyOver;
end

% Bombing = log10 (Bombing); %
CSR = 0.1;
Bombing (tmesh+1) =0;

subplot (1, 2, 2),
plot ([0 Bombing (1)], [Y (1) Y (1)]);
hold on;
serration = 0;
TotalBomb = 0;
for k = 1: tmesh
   TotalBomb = TotalBomb + Bombing (k) * (Y (k+1)-Y (k));
   if (Bombing (k) < 1/CSR)
      plot ([Bombing (k) Bombing (k)], [Y (k) Y (k+1)], 'r-o');
      serration = serration + (Y (k+1)-Y (k));
   else
      plot ([Bombing (k) Bombing (k)], [Y (k) Y (k+1)], 'b-o');
   end
   plot ([Bombing (k) Bombing (k+1)], [Y (k+1) Y (k+1)], 'k');
end
xlabel ('Visit Intensity');

% sum rule: TotalBomb should be equal to max (t)-min (t) %
fprintf (1,'TotalBomb = %g (%g) seconds\n', TotalBomb, max (t)-min (t));
```

```
% This is the average strain rate reciprocal %
AvgBombing = TotalBomb / (Y (tmesh+1)-Y (1));
fprintf (1,'AvgBombing = %g second per 100%%\n', AvgBombing);
fprintf (1,'1/CSR = %g second per 100%%; ratio to AvgBombing = %g\n', ...
            1/CSR, 1/AvgBombing/CSR);

Controllability =-log(1-serration/(Y (tmesh+1)-Y (1)));

plot ([1/CSR 1/CSR], [Y (1) Y (tmesh+1)], 'r:');
plot ([AvgBombing AvgBombing], [Y (1) Y (tmesh+1)], 'g--');
grid on;
axis ([0 1.2*AvgBombing/Controllability min (ep) max (ep)]);

fprintf (1, 'Controllability = %g\n', Controllability);

print -djpeg TimeBasedControllability.jpg;
```

2 Supplementary figures

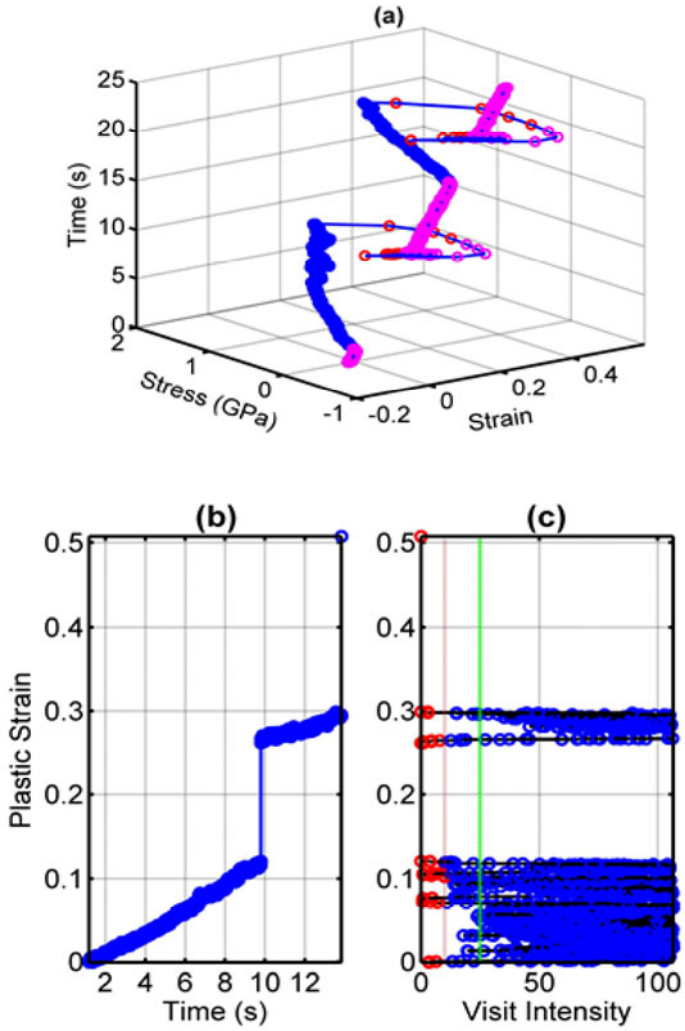

Figure S1 CI calculation for the D=210 nm single-crystal Al pillar. The blue ones are the useful data. The red ones are ‘‘too fast’’ data. The purple ones are the ‘‘empty load’’ data. (a) Strain-stress-time curve; (b) plastic strain-time curve; (c) visit intensity at each plastic strain range.

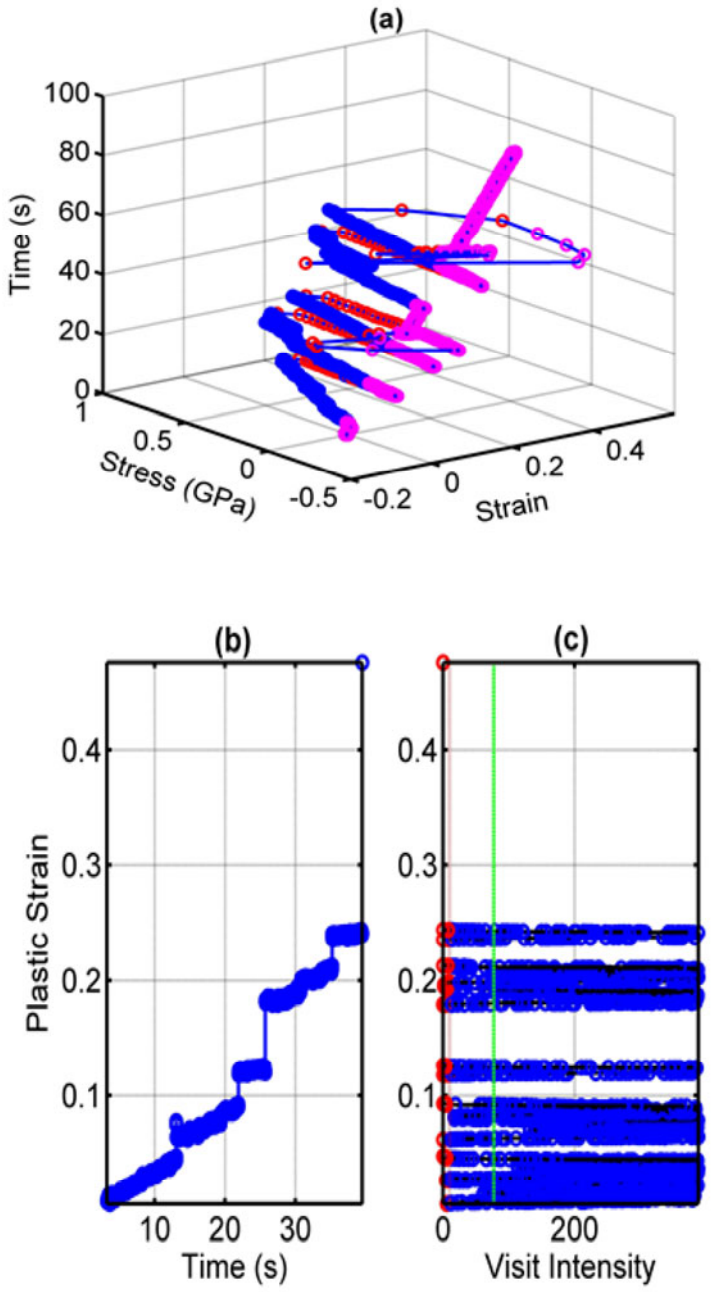

Figure S2 CI calculation of the *D*=406 nm single-crystal Al pillar. The color scheme is the same as in Figure S1. (a) Strain-stress-time curve; (b) plastic strain-time curve; (c) visit intensity at each plastic strain range.

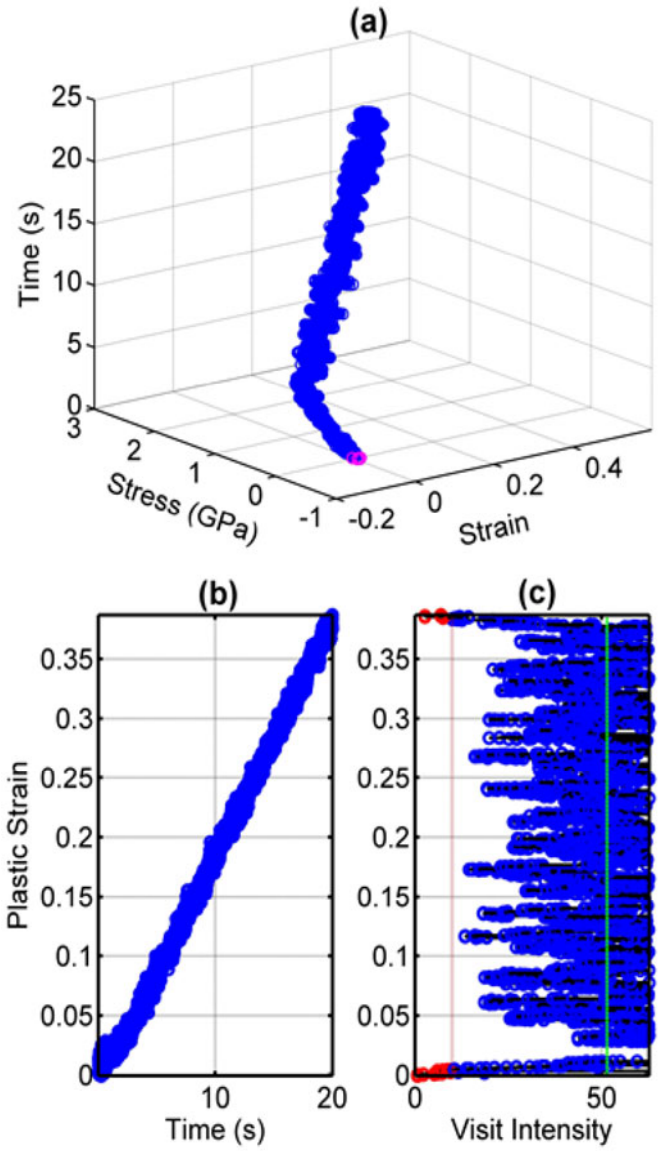

Figure S3 CI calculation of the D=108 nm polycrystalline Al nanopillar. The color scheme is the same as in Figure S1. (a) Strain-stress-time curve; (b) plastic strain-time curve; (c) visit intensity at each plastic strain range.

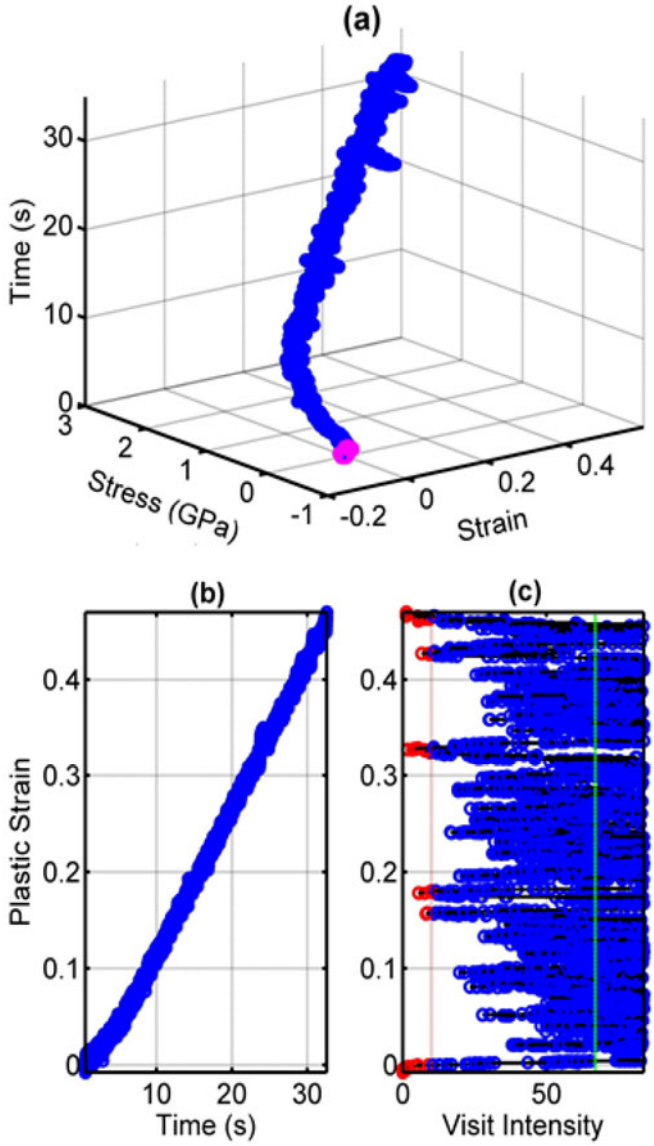

Figure S4 CI calculation of the D=141 nm polycrystalline Al nanopillar. The color scheme is the same as in Figure S1. (a) Strain-stress-time curve; (b) plastic strain-time curve; (c) visit intensity at each plastic strain range.